Crystalline electric field of the bromo-elpasolites Cs_2NaRBr_6 (R=rare earth) determined by inelastic neutron scattering

Albert Furrer
Laboratorium für Neutronenstreuung, Eidgenössische Technische Hochschule Zürich and Paul Scherrer Institut, CH-5232 Villigen PSI, Switzerland

Hans-Ueli Güdel
Institut für Anorganische Chemie, Universität Bern, Freiestrasse 3, CH-3000 Bern 9, Switzerland
(Received 20 May 1997; revised manuscript received 12 September 1997)

The rare-earth based bromo-elpasolites Cs_2NaRBr_6 (R=Ce, Pr, Nd, Tb, Dy, Ho, Er, Tm, Yb) were synthesized and subsequently studied by inelastic neutron scattering. Energy splittings within the electronic ground-state J multiplet due to the crystalline electric field (CEF) interaction at the R^{3+} site were directly observed and rationalized in terms of CEF parameters of cubic symmetry. For some CEF transitions we have been able to resolve the splitting due to the tetragonal distortion. The resulting CEF parameters are discussed and used to predict some properties of the long-range magnetic ordering at low temperatures. [S0163-1829(97)03748-X]

I. INTRODUCTION

The crystalline electric field (CEF) interaction has been shown to have considerable influence on the magnetic properties of rare-earth compounds. This is particularly true for systems with small magnetic ordering temperatures or for systems that do not order magnetically at all. The elpasolites Cs_2NaRBr_6 (R=rare earth) belong to this category. They all have a cubic crystal structure, space group $Fm3m$ (O_h^5), with the R^{3+} ions situated at sites of exact octahedral (O_h) symmetry, i.e., each R^{3+} ion is hexacoordinated by six nearest Br^- ions, see Fig. 1. The elpasolites are therefore good candidates for a systematic study of CEF effects. They all show transitions to distorted variants of the elpasolite structure on lowering the temperature. The distortions can be represented as small rotations of the RBr_6 octahedra about the fourfold axis of the crystal, giving rise to a tetragonal crystal structure with symmetry C_{4h} at the R^{3+} sites. The relevant structural properties of the elpasolites Cs_2NaRBr_6 are summarized in Table I. The separation between nearest-neighbor R^{3+} ions corresponds to $(\sqrt{2}/2)a$ (where a is the lattice parameter), which is so large that direct exchange coupling is expected to be extremely small. In addition, the RBr_6^{3-} units can be considered as molecular units, because there are no bromide bridges between neighboring R^{3+} ions that would provide a convenient superexchange pathway. The magnetic coupling between the R^{3+} ions is then predominantly of dipolar origin, and very low magnetic ordering temperatures may be expected. Magnetic order due to dipolar forces is of continued interest in the study of magnetism, because the dipolar Hamiltonian is known exactly. With these considerations in mind we investigated the CEF of the elpasolites Cs_2NaRBr_6 in detail by the inelastic neutron-scattering (INS) technique in order to set a basis for future studies of their low-temperature magnetic properties.

Another motivation for the present work emerged from ongoing studies of the related compounds $Cs_3R_2Br_9$ for which we are interested in the nature of the magnetic coupling within the dimeric R^{3+} units.[1–5] The R^{3+} site symmetry of the $Cs_3R_2Br_9$ compounds is similar to the elpasolites Cs_2NaRBr_6, i.e., the $Cs_3R_2Br_9$ compounds contain $R_2Br_9^{3-}$ dimers of two face-sharing RBr_6^{3-} octahedra as discrete units. For the understanding of the magnetic excitation spectra of the $Cs_3R_2Br_9$ compounds it is therefore important to know the CEF interaction in the absence of exchange, and this is achieved by studying the elpasolites Cs_2NaRBr_6.

The magnetic properties of the elpasolites Cs_2NaRBr_6 are practically unexplored. Some room-temperature structural properties have been reported in connection with the successful synthesis of these ternary compounds.[6,7] A preliminary neutron spectroscopic investigation of the CEF has been reported for R=Nd, Tb, and Yb.[8] High-resolution optical spectroscopy has been used to determine CEF splittings in Cs_2NaRBr_6 (R=Tb, Ho, Tm, Yb) as well as in Pr^{3+}-doped Cs_2NaYBr_6 and Yb^{3+}-doped $Cs_2NaHoBr_6$.[9,10] Some thermodynamic properties and features of the phonon dispersion have been presented for R=Dy, Ho, and Tm,[11,12] focusing

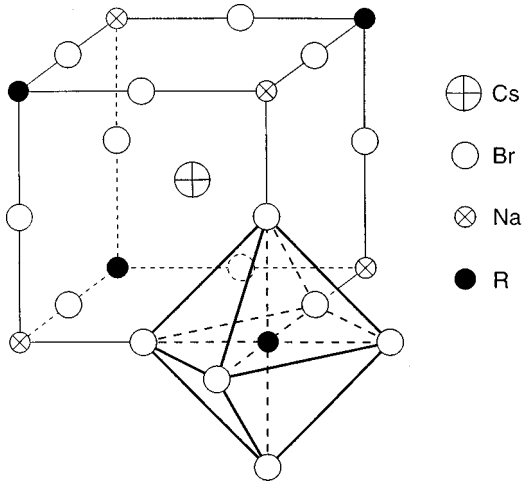

FIG. 1. An octant of the unit cell of the Cs_2NaRBr_6 elpasolite lattice.

 © 1997 The American Physical Society

TABLE I. Lattice parameters a at room temperature and temperatures T_t of the cubic-to-tetragonal phase transition of the Cs_2NaRBr_6 compounds.

R	a (pm)[a]	T_t (K)
La	1151.9	316[a]
Ce	1150.3	288[a]
Pr	1146.8	256[a]
Nd	1144.6	238[a]
Sm	1139.3	198[a]
Eu	1137.8	183[a]
Gd	1136.1	173[a]
Tb	1133.4	
Dy	1131.4	139[b]
Ho	1129.3	126[b]
Er	1127.9	
Tm	1125.3	101[b]
Yb	1124.5	≈80[c]

[a]Reference 6.
[b]Reference 12.
[c]Reference 8.

mainly on the cubic-to-tetragonal phase transition. The structurally related elpasolite series Cs_2NaRCl_6, on the other hand, has been investigated by a number of experimental techniques. Energy splittings resulting from CEF interactions were derived from magnetic susceptibility measurements[13,14] as well as optical,[15–17] Raman,[18,19] and neutron[8] spectroscopy. There is general agreement about the relative order of the CEF levels and the nature of the ground level, although the size of the CEF splitting differs by factors of up to 4 in some cases. In terms of CEF theory it was shown that the point-charge model is completely inadequate and covalency effects are important.[20] An attempt to clarify both the experimental and theoretical situation resulted in a rather consistent CEF data set.[21,22] Recent measurements of the magnetic susceptibility revealed long-range ferromagnetic ordering for R=Gd, Dy, and Er below T_c=35, 21, and 50 mK, respectively,[23] which clearly indicates that dipolar forces are controlling the magnetic coupling between the R^{3+} ions.

The present paper is organized as follows. In Sec. II we summarize the symmetry aspects of the CEF interaction in the Cs_2NaRBr_6 compounds. Section III provides a brief introduction into the INS technique applied to the measurements of CEF splittings. Experimental aspects are given in Sec. IV. The experimental results and the data analysis are presented in Sec. V, and in Sec. VI we discuss our results and give some final conclusions.

II. THE CRYSTALLINE ELECTRIC FIELD

The mathematical problem which has to be solved is the calculation of the electrostatic potential at the R^{3+} ion position which is given by

$$V_{\mathrm{CEF}}(\mathbf{r})=\sum_i \frac{\rho(\mathbf{R}_i)}{|\mathbf{r}-\mathbf{R}_i|}, \tag{1}$$

where $\rho(\mathbf{R}_i)$ denotes the charge distribution at the site $\mathbf{R}_i$ of the ith ligand ion. Equation (1) can be expanded in terms of spherical harmonics Y_n^m. Stevens introduced the operator equivalents method[24] in which products of Cartesian coordinates x, y, and z are essentially replaced by corresponding combinations of total angular momentum operators J_x, J_y, and J_z. In this way, an effective spin operator is formed with the same transformation properties under rotation as the CEF potential (1). For cubic symmetry O_h and the polar axis along the cube edge the corresponding Hamiltonian is given by[25]

$$H_{\mathrm{CEF}}(O_h)=B_4(O_4^0+5O_4^4)+B_6(O_6^0-21O_6^4), \tag{2}$$

where the B_n denote the CEF parameters and the O_n^m are Stevens's operator equivalents.[24] The eigenvalues and eigenvectors of Eq. (2) were tabulated by Lea, Leask, and Wolf[26] for all R^{3+} ions and for all possible ratios B_4/B_6.

All the elpasolites Cs_2NaRBr_6 are known to undergo a cubic-to-tetragonal phase transition, see Table I. The CEF Hamiltonian for tetragonal symmetry C_{4h} reads

$$H_{\mathrm{CEF}}(C_{4h})=B_2^0O_2^0+B_4^0O_4^0+B_4^4O_4^4+B_6^0O_6^0+B_6^4O_6^4. \tag{3}$$

For small tetragonal deformations $t=(c-a)/a\ll 1$, Eq. (3) can be approximated as[27]

$$H_{\mathrm{CEF}}(C_{4h})=B_2^0O_2^0+B_4[(1-\tfrac{10}{7}t)O_4^0+5O_4^4]+B_6[(1-\tfrac{28}{3}t)O_6^0-21O_6^4]. \tag{4}$$

For the Cs_2NaRBr_6 compounds we have $t\approx 0.008$,[7] so that Eq. (4) clearly applies.

In rare-earth compounds the CEF interaction is usually much smaller than the spin-orbit interaction, so that the total angular momentum J is a good quantum number and admixtures of states in different J multiplets can be neglected. This is particularly true for the elpasolites Cs_2NaRBr_6 (in contrast, e.g., to the rare-earth based cuprate high-temperature superconductors), so that the above treatment of the CEF interaction in terms of a perturbation of the ground-state J multiplet alone is fully justified.

III. INELASTIC NEUTRON SCATTERING

The CEF interaction discussed in Sec. II gives rise to discrete energy levels E_i that can be spectroscopically determined by the INS technique. For a system of N noninteracting ions the thermal-neutron cross section for the CEF transition $\Gamma_i\rightarrow\Gamma_j$ is given in the dipole approximation by[28]

$$\frac{d^2\sigma}{d\Omega\, d\omega}=\frac{N}{Z}\left(\frac{\gamma e^2}{m_e c^2}\right)^2\frac{k_1}{k_0}\exp\{-2W\}F^2(Q)\times\exp\left\{-\frac{E_i}{k_BT}\right\}|\langle\Gamma_j|J_p|\Gamma_i\rangle|^2\,\delta(E_i-E_j\pm\hbar\omega), \tag{5}$$

where $\exp\{-2W\}$ is the Debye-Waller factor, $F(Q)$ the magnetic form factor, J_p the component of the total angular momentum operator perpendicular to the scattering vector $\mathbf{Q}$, and $\hbar\omega$ the energy transfer. The remaining symbols have their usual meaning. Some of the transition matrix elements $\langle\Gamma_j|J_p|\Gamma_i\rangle$ are zero by symmetry, thus leading to strict selection rules for INS transitions. The transition matrix ele-

ments were tabulated by Birgeneau[29] for all R^{3+} ions with cubic site symmetry and for all possible ratios B_4/B_6.

One problem remains, namely, the question of whether peaks observed in the energy spectra really arise from CEF transitions or whether they result, say, from phonon scattering. However, CEF transitions may be distinguished from phonon processes by the way in which the intensities vary with temperature and momentum transfer. With increasing modulus of the scattering vector **Q** the CEF intensity decreases according to $F^2(Q)$ as can be seen from the cross-section formula (5), whereas the phonon peak intensity usually increases with Q^2 (apart from the modulation due to the structure factor). Furthermore, phonons obey Bose statistics, whereas the population of CEF levels is governed by Boltzmann statistics.

IV. EXPERIMENT

The procedures given in Ref. 7 were used for the synthesis of the Cs_2NaRBr_6 compounds. The starting materials all had a nominal purity of 99.9% or better. Some samples were grown as single crystals by the Bridgman technique. Starting materials were either the corresponding polycrystalline materials, prepared according to Ref. 7, or a stoichiometric mixture of the binary halides. The compounds were checked by powder x-ray diffraction and (in part) by powder neutron diffraction. Impurity contents were less than 1%.

All the INS measurements were carried out at the reactor Saphir of the Paul Scherrer Institute at Villigen/Würenlingen with use of a triple-axis spectrometer in the neutron energy-loss configuration. The energy of the scattered neutrons was kept fixed either at 5.0, 13.7, or 15.0 meV, giving rise to energy resolutions (at $\hbar\omega=0$) of 0.2, 1.1, or 1.2 meV, respectively. For $\hbar\omega>0$ the energy resolution becomes increasingly worse. To gain intensity the measurements were carried out with use of a doubly bent graphite monochromator as well as a horizontally bent graphite analyzer, both with (002) scattering planes. Consequently, no collimations were used from neutron source to detector. Pyrolitic graphite or beryllium filters were inserted into the outgoing neutron beam to reduce higher-order contamination. The samples were sealed in aluminum cylinders of 10–15 mm diameter and 50 mm length and mounted in a closed-cycle helium refrigerator to achieve temperatures $T\geqslant 8$ K.

V. RESULTS AND DATA ANALYSIS

In the following subsections we present representative CEF spectra obtained for the Cs_2NaRBr_6 compounds by the INS technique. In addition to the energy spectra shown in the present paper, we have performed numerous studies of the Q and T dependence of the CEF transitions in order to verify the magnetic origin of the scattering as predicted by the cross-section formula (5). In the data analysis the following procedure was adopted.

(1) The inelastic lines associated with the CEF transitions were fitted to Gaussian functions above a linear background.

(2) The peak positions as well as the temperature dependence of the peak intensities were used to set up the CEF level schemes. The results for all studied compounds are summarized in Fig. 2.

(3) A least-squares fitting procedure was applied to each CEF level scheme in order to derive the CEF parameters. These calculations were performed throughout for cubic site symmetry O_h, with the eigenvalues of Eq. (2) expressed in terms of the CEF parameters B_4 and B_6. The splitting due to the tetragonal distortion is rather small for the elpasolites Cs_2NaRBr_6 and could not be resolved experimentally except for a few transitions. In these cases the position of the CEF state was set equal to the weighted average of the tetragonally split CEF levels. The starting values of the CEF parameters were those of the corresponding Cs_2NaRCl_6 series.[8,21] The best-fitted CEF parameters are listed in Table II.

(4) The reliability of the resulting CEF parameters was checked by comparing the observed and calculated intensities of the CEF transitions according to the cross-section formula (5). In fact, the agreement was usually better than 10% as demonstrated for some cases.

(5) In those cases where we have been able to observe additional splittings of CEF transitions due to the tetragonal distortion, we have derived the tetragonal CEF parameter by varying B_2^0 according to Eq. (4) until the best agreement was achieved between the observed and calculated energies and intensities of the corresponding tetragonally split CEF transitions. The resulting parameters B_2^0 are listed in Table II.

A. $Cs_2NaLaBr_6$

Energy spectra were taken for nonmagnetic $Cs_2NaLaBr_6$ in order to obtain an insight into the amount of phonon scattering that is naturally present also in the magnetic compounds. As shown in Fig. 3 there is considerable phonon scattering centered at around 6, 18, and 38 meV. Above 40 meV we have a sloping background due to the increasing measuring time. The phonon scattering is weak, typically two neutron counts per min. As we will see in the following subsections, the intensities associated with the CEF transitions usually exceed the phonon count rates by an order of magnitude at least, thus we can neglect phonon scattering in most cases. However, when the CEF transition matrix elements are small (particularly for high-energy CEF transitions), we have to take care of phonons in the interpretation of the observed energy spectra. Care is also necessary for $Cs_2NaYbBr_6$ where the phonon scattering is strongly enhanced as a result of the large nuclear scattering length of Yb^{3+}. In all the energy spectra presented in Sec. V, phonon scattering is indicated by the letter P from Fig. 3 to Fig. 15.

B. $Cs_2NaCeBr_6$

The cubic CEF splits the sixfold-degenerate ground-state multiplet $^2F_{5/2}$ of the Ce^{3+} ion into a doublet Γ_7 and a quartet Γ_8. The energy spectra observed for $Cs_2NaCeBr_6$ exhibit a series of inelastic lines below 50 meV that, by comparison with nonmagnetic $Cs_2NaLaBr_6$, can be interpreted as phonon scattering (see Fig. 3). However, $Cs_2NaCeBr_6$ shows an additional peak A at 59 meV that is absent for $Cs_2NaLaBr_6$, thus it can readily be assigned to the CEF transition $\Gamma_7\rightarrow\Gamma_8$.

C. $Cs_2NaPrBr_6$

The cubic CEF splits the ninefold-degenerate ground-state multiplet $^3H_4$ of the Pr^{3+} ion into a singlet Γ_1, a doublet

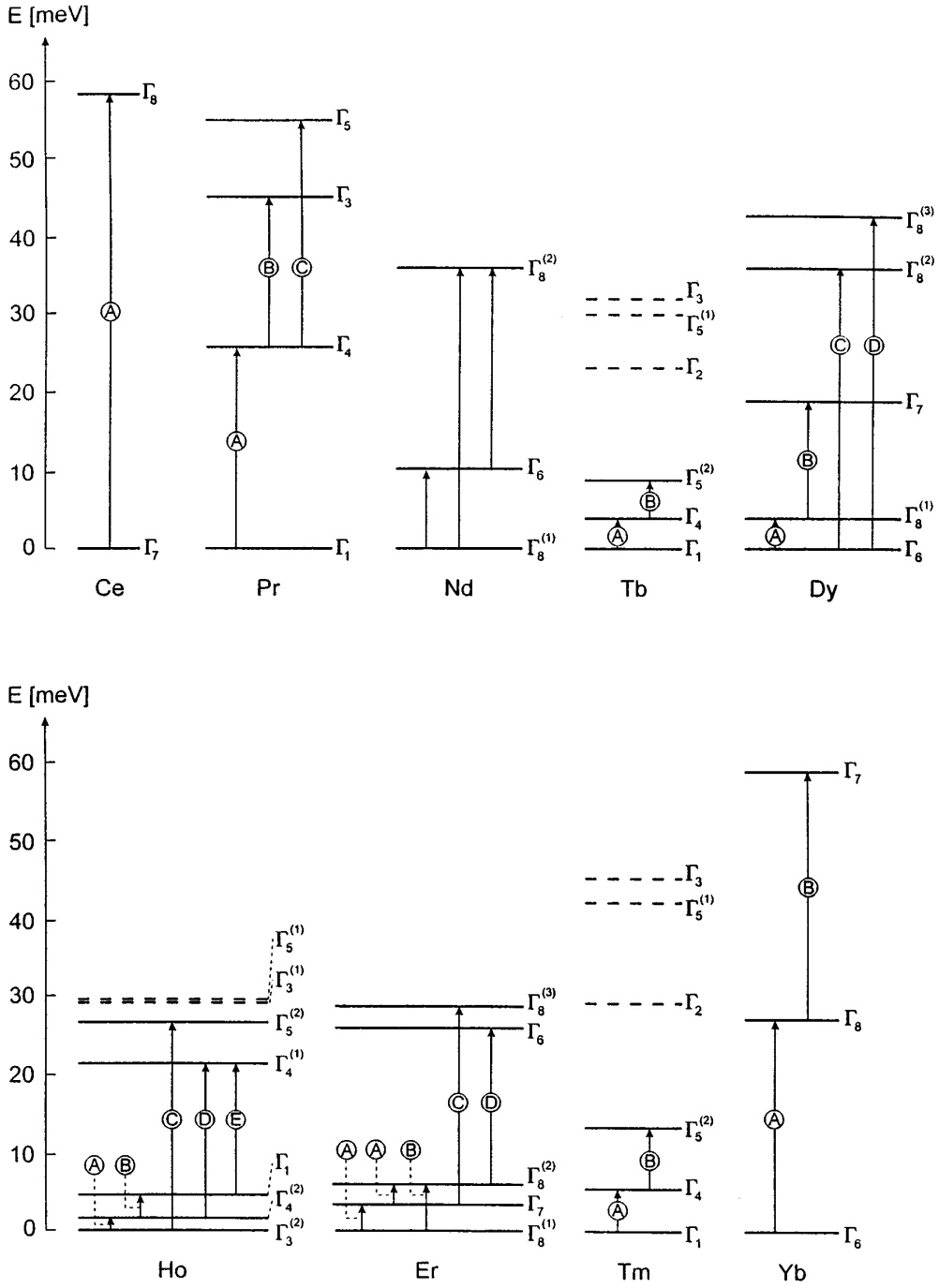

FIG. 2. CEF energy-level schemes of the elpasolites Cs_2NaRBr_6 derived in the present work. The full lines correspond to the CEF levels measured directly by INS experiments. Calculated CEF states are indicated by dashed lines. The arrows and corresponding labels denote the observed CEF transitions, see Fig. 3 to Fig. 15.

Γ_3, and two triplets Γ_4 and Γ_5. All CEF transitions are allowed between the three states Γ_3, Γ_4, and Γ_5, whereas for the singlet only the $\Gamma_1 \rightarrow \Gamma_4$ transition is allowed. Energy spectra taken at $T = 10$ K give evidence for only one CEF transition at 25 meV (peak A) which we can therefore identify as the $\Gamma_1 \rightarrow \Gamma_4$ transition, see Fig. 4. Upon heating to $T = 150$ K the intensity of peak A decreases according to the Boltzmann population factor, but two further inelastic lines B and C show up at 18 and 30 meV, respectively, which correspond to CEF excitations out of the first-excited Γ_4 state. The observed reduction of all the peak intensities by 20% upon increasing Q from 2.7 to 3.7 Å^{-1} is in perfect agreement with the corresponding decrease of the magnetic form factor $F(Q)$, which therefore clearly confirms the CEF origin of the inelastic lines. Since the energy of the $\Gamma_4 \rightarrow \Gamma_3$ transition is always $\frac{5}{7}$ of the energy of the $\Gamma_1 \rightarrow \Gamma_4$ transition,[26] peak B can readily be attributed to the $\Gamma_4 \rightarrow \Gamma_3$ transition. Peak C can then be identified as the $\Gamma_4 \rightarrow \Gamma_5$ transition. This interpretation is furthermore confirmed by the observed intensity ratio $I_B/I_C = 2.3 \pm 0.5$ which is predicted to be 2.6 from the CEF model. The CEF level scheme is therefore completely determined.

TABLE II. CEF parameters of the elpasolites Cs_2NaRBr_6 determined in the present work.

R	B_2^0 (meV)	B_4 (meV)	B_6 (meV)
Ce	>0*	0.162 ± 0.002	0
Pr	>0*	$(-1.32\pm0.06)\times10^{-2}$	$(1.39\pm0.13)\times10^{-4}$
Nd	>0*	$(-7.6\pm0.2)\times10^{-3}$	$(-7.2\pm0.3)\times10^{-5}$
Tb	>0*	$(2.1\pm0.2)\times10^{-3}$	$(-1.5\pm0.4)\times10^{-6}$
Dy	$(1.5\pm0.2)\times10^{-2}$	$(-1.3\pm0.1)\times10^{-3}$	$(1.5\pm0.3)\times10^{-6}$
Ho	$(3.0\pm0.8)\times10^{-3}$	$(-6.2\pm0.5)\times10^{-4}$	$(-1.4\pm0.2)\times10^{-6}$
Er	<0*	$(8.1\pm0.3)\times10^{-4}$	$(1.8\pm0.1)\times10^{-6}$
Tm	<0*	$(3.0\pm0.4)\times10^{-3}$	$(-4.2\pm0.8)\times10^{-6}$
Yb	<0*	$(-3.1\pm0.1)\times10^{-2}$	$(1.1\pm0.3)\times10^{-4}$

*Expected sign of B_2^0, see Sec. VI.

D. $Cs_2NaNdBr_6$

The cubic CEF splits the tenfold-degenerate ground-state multiplet $^4I_{9/2}$ of the Nd^{3+} ion into a doublet Γ_6 and two quartets $\Gamma_8^{(1)}$ and $\Gamma_8^{(2)}$. In an earlier INS experiment[8] we have been able to unambiguously determine the CEF level scheme with $\Gamma_8^{(2)}$ being the ground state and Γ_6 and $\Gamma_8^{(1)}$ the excited states at 10 and 36 meV, respectively.

E. $Cs_2NaTbBr_6$

The cubic CEF splits the 13-fold-degenerate ground-state multiplet $^7F_6$ of the Tb^{3+} ion into two singlets Γ_1 and Γ_2, a doublet Γ_3, and three triplets Γ_4, $\Gamma_5^{(1)}$, and $\Gamma_5^{(2)}$. As in all terbium compounds with O_h coordination, the singlet Γ_1 was found to be the ground state. In fact, at low temperature ($T=10$ K) only one inelastic line at 4 meV (peak A) is observed (see Fig. 5) which is attributed to the $\Gamma_1\rightarrow\Gamma_4$ transition (which is the only allowed transition out of the Γ_1 state). The marginal shoulder at 5 meV (peak B) corresponds to an excited CEF transition whose intensity increases at higher temperature as expected. Note that in our earlier work[8] the excited CEF transition B was erroneously attributed to the phonon line at 6.5 meV, which resulted in a wrong set of CEF parameters. Attempts to locate higher excited CEF states failed, since due to small transition probabilities and/or thermal population factors the weak CEF signals could not be distinguished unambiguously from the phonon scattering. Nevertheless, the observation of two excited CEF levels is sufficient to determine the two CEF parameters B_4 and B_6. The calculated energies of the CEF levels at higher energies are included in Fig. 2.

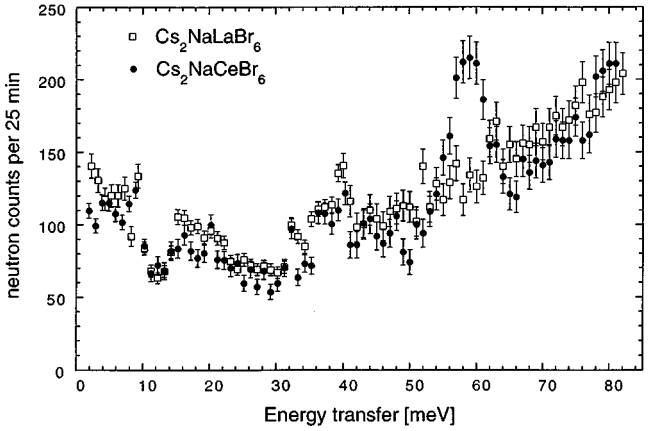

FIG. 3. Energy spectra of neutrons scattered from $Cs_2NaLaBr_6$ and $Cs_2NaCeBr_6$. $E_A=13.7$ meV, $T=10$ K, $Q=2.8$ Å^{-1} for $\hbar\omega\leqslant40$ meV and $Q=4.5$ Å^{-1} for $\hbar\omega\geqslant41$ meV.

F. $Cs_2NaDyBr_6$

The cubic CEF splits the 16-fold-degenerate ground-state multiplet $^6H_{15/2}$ of the Dy^{3+} ion into two doublets Γ_6 and Γ_7 and three quartets $\Gamma_8^{(1)}$, $\Gamma_8^{(2)}$, and $\Gamma_8^{(3)}$. Figure 6 shows the low-energy part of the CEF spectrum with an intense line A_1 at 3 meV and a shoulder A_2 at 5 meV which corresponds to the $\Gamma_6\rightarrow\Gamma_8^{(1)}$ transition. The $\Gamma_8^{(1)}$ quartet is clearly split into two doublets due to the tetragonal distortion. The second-

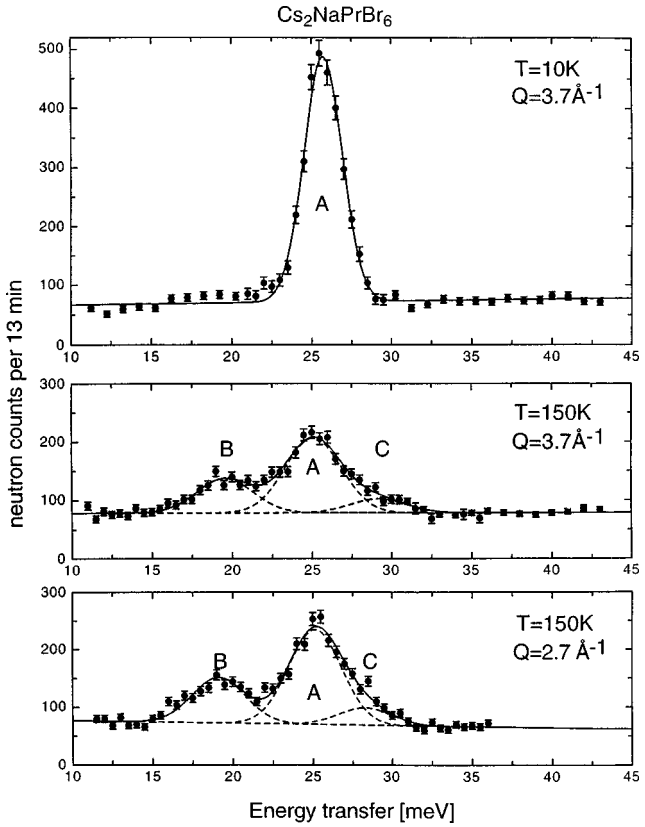

FIG. 4. Energy spectra of neutrons scattered from $Cs_2NaPrBr_6$. $E_A=15$ meV, $Q=3.7$ Å^{-1}.

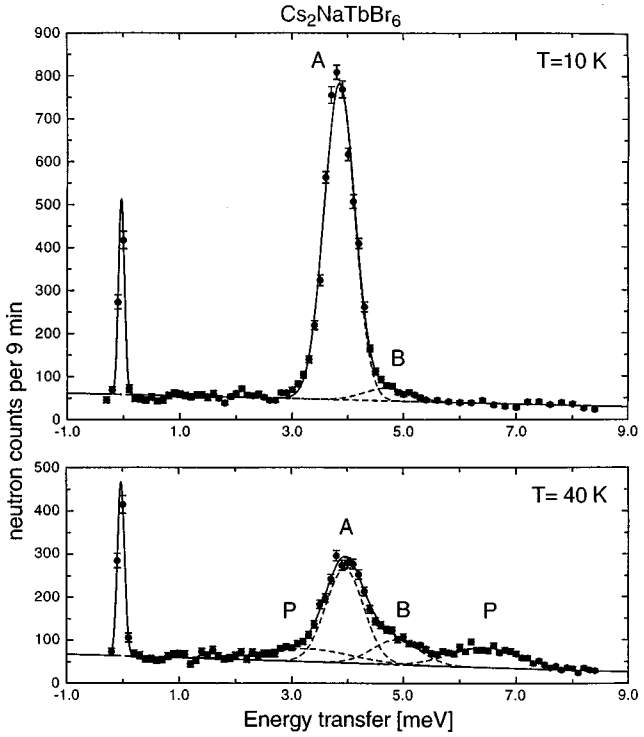

FIG. 5. Low-energy spectra of neutrons scattered from $Cs_2NaTbBr_6$. $E_A = 5$ meV, $Q = 1.2$ Å^{-1}.

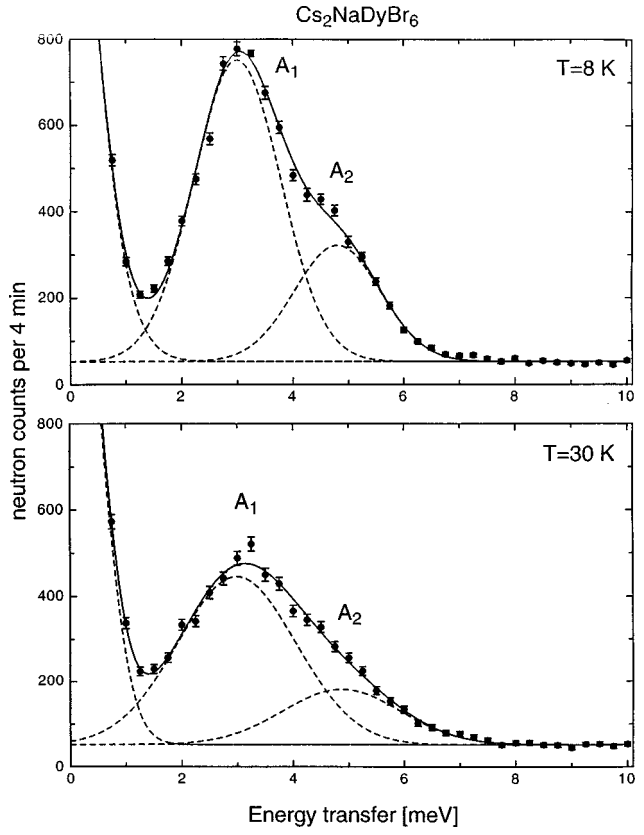

FIG. 6. Low-energy spectra of neutrons scattered from $Cs_2NaDyBr_6$. $E_A = 15$ meV, $Q = 1.3$ Å^{-1}.

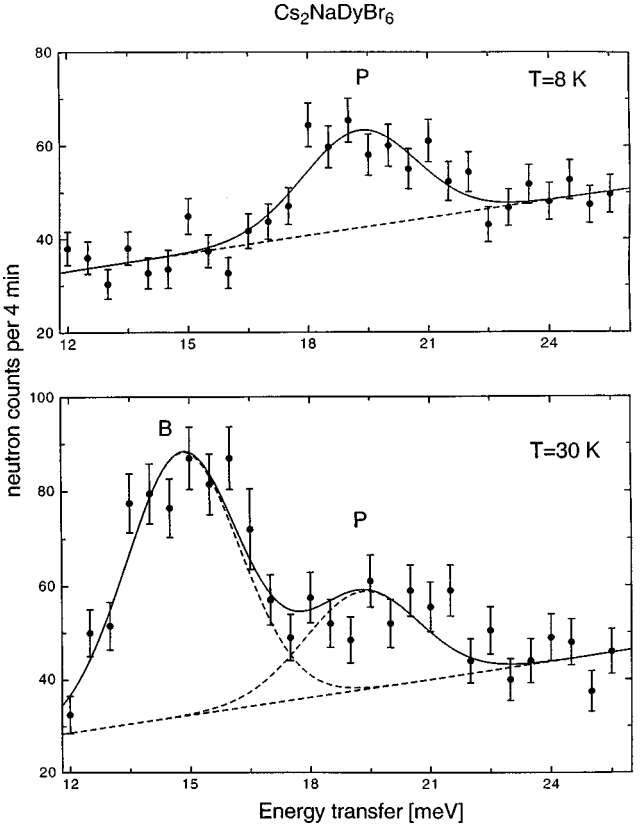

FIG. 7. Medium-energy spectra of neutrons scattered from $Cs_2NaDyBr_6$. $E_A = 15$ meV, $Q = 2.1$ Å^{-1}.

excited CEF state is the Γ_7 doublet. However, the $\Gamma_6 \rightarrow \Gamma_7$ ground-state transition is forbidden; thus the energy of the Γ_7 doublet can only be determined by an excited-state transition. This is demonstrated in Fig. 7 where the line at 19 meV corresponds to phonon scattering. Upon raising the temperature from 8 to 30 K, the phonon scattering remains unaffected, but the first-excited CEF state is now sufficiently populated to give rise to the $\Gamma_8^{(1)} \rightarrow \Gamma_7$ transition at 15 meV (peak B). Figure 8 shows the ground-state CEF transitions to the two high-lying CEF states, which have rather small transition probabilities. Thus the CEF level scheme is completely determined. In the data interpretation we have been able to derive the tetragonal CEF parameter B_2^0 from the observed

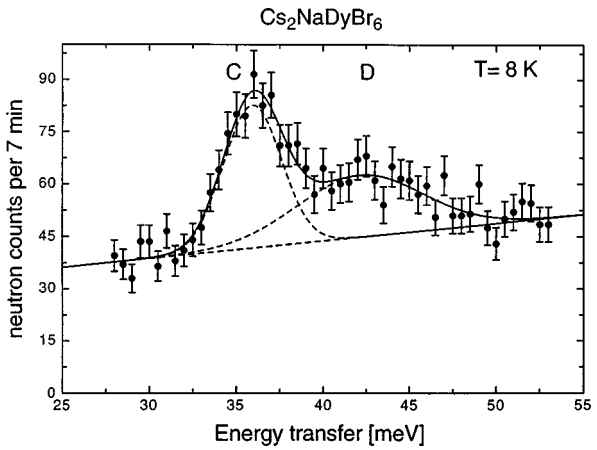

FIG. 8. High-energy spectrum of neutrons scattered from $Cs_2NaDyBr_6$. $E_A = 13.7$ meV, $Q = 3.6$ Å^{-1}.

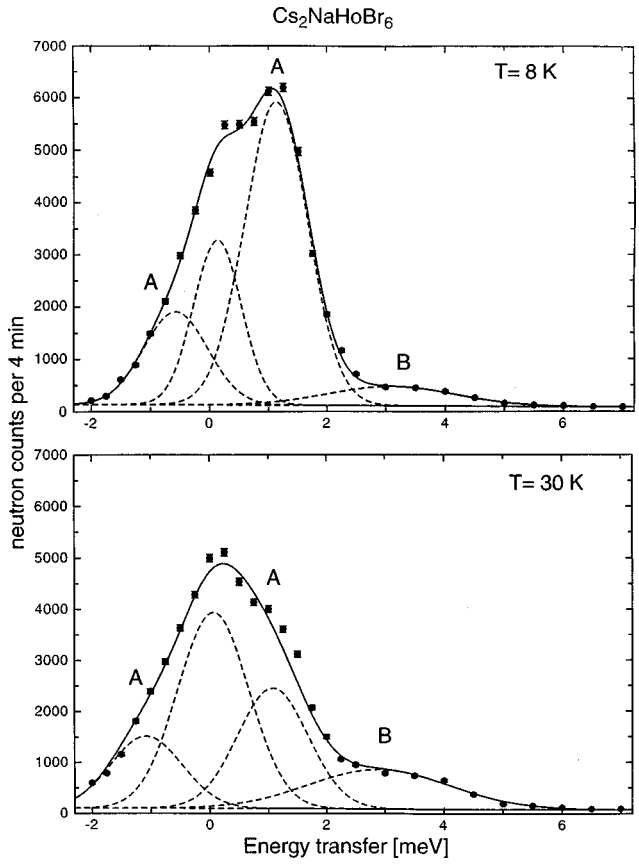

FIG. 9. Low-energy spectra of neutrons scattered from $Cs_2NaHoBr_6$. $E_A = 13.7$ meV, $Q = 1.5$ Å^{-1}.

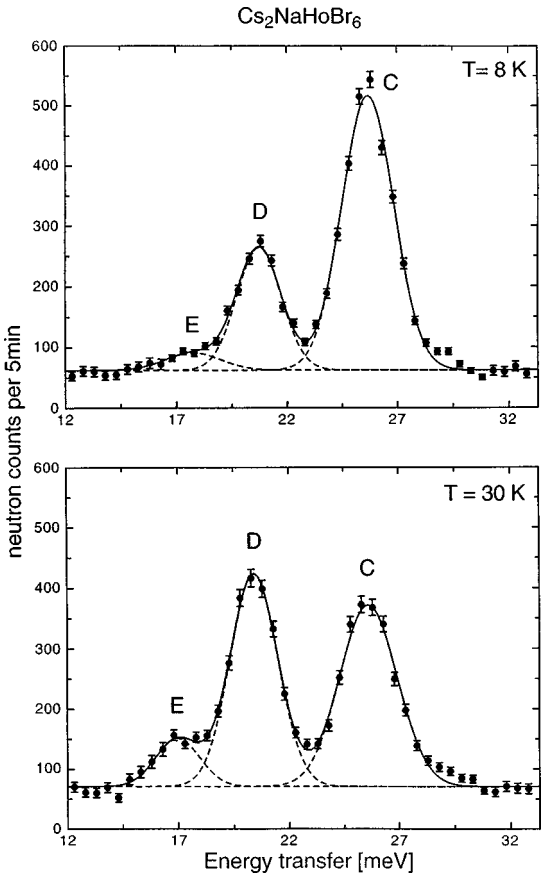

FIG. 10. Medium- and high-energy spectra of neutrons scattered from $Cs_2NaHoBr_6$. $E_A = 13.7$ meV, $Q = 2.7$ Å^{-1}.

splitting of the $\Gamma_6 \rightarrow \Gamma_8^{(1)}$ transition, see Fig. 6. The tetragonal splitting of the highest $\Gamma_8^{(2)}$ and $\Gamma_8^{(3)}$ quartets is much smaller and could not be resolved.

G. $Cs_2NaHoBr_6$

The cubic CEF splits the 17-fold-degenerate ground-state multiplet $^5I_8$ into a singlet Γ_1, two doublets $\Gamma_3^{(1)}$ and $\Gamma_3^{(2)}$, and four quartets $\Gamma_4^{(1)}$, $\Gamma_4^{(2)}$, $\Gamma_5^{(1)}$, and $\Gamma_5^{(2)}$. Figure 9 shows the low-energy part of the CEF spectrum. There is a huge inelastic line at 1 meV (peak *A*), which shows up in both the energy-gain and the energy-loss configuration. In the latter configuration its intensity is decreasing with increasing temperature; thus it can readily be attributed to the ground-state CEF transition $\Gamma_3^{(2)} \rightarrow \Gamma_4^{(2)}$. The second inelastic line (peak *B*) at 3 meV, exhibiting the opposite intensity behavior with temperature, corresponds to the excited-state $\Gamma_4^{(2)} \rightarrow \Gamma_1$ transition. At higher energies three further CEF states (peaks *C*, *D*, and *E*) can be located as indicated in Fig. 10. Again, the temperature dependence nicely demonstrates whether the observed CEF transitions occur out of the ground state or out of excited states; thus the CEF energy-level sequence could be reconstructed in a straightforward manner as shown in Fig. 2. The two highest CEF levels $\Gamma_3^{(1)}$ and $\Gamma_5^{(1)}$ could not be observed because of the extremely small matrix elements associated with transitions out of the three lowest CEF states. Nevertheless, their calculated energies are included in Fig. 2.

The lowest CEF transition $\Gamma_3^{(2)} \rightarrow \Gamma_4^{(2)}$ was measured with increased energy resolution, see Fig. 11. We clearly observe a decomposition into three inelastic lines due to the tetragonal distortion which splits both the ground-state doublet $\Gamma_3^{(2)}$

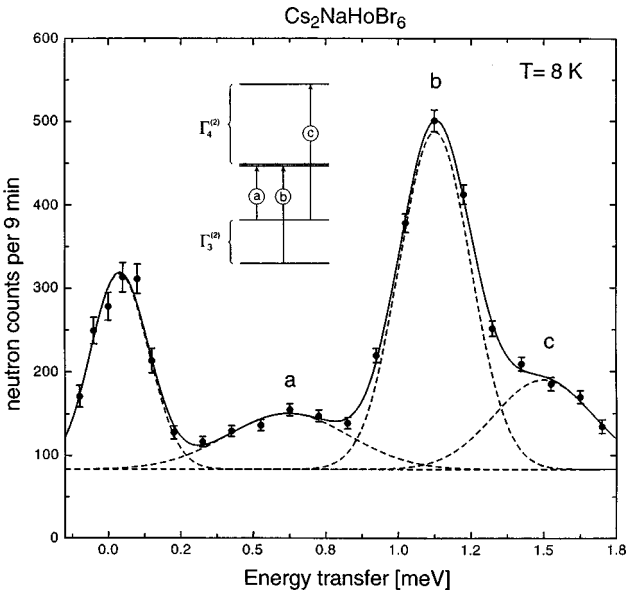

FIG. 11. High-resolution low-energy spectrum of neutrons scattered from $Cs_2NaHoBr_6$. $E_A = 5$ meV, $Q = 0.8$ Å^{-1}. The inset shows the tetragonal splitting of the low-lying CEF levels.

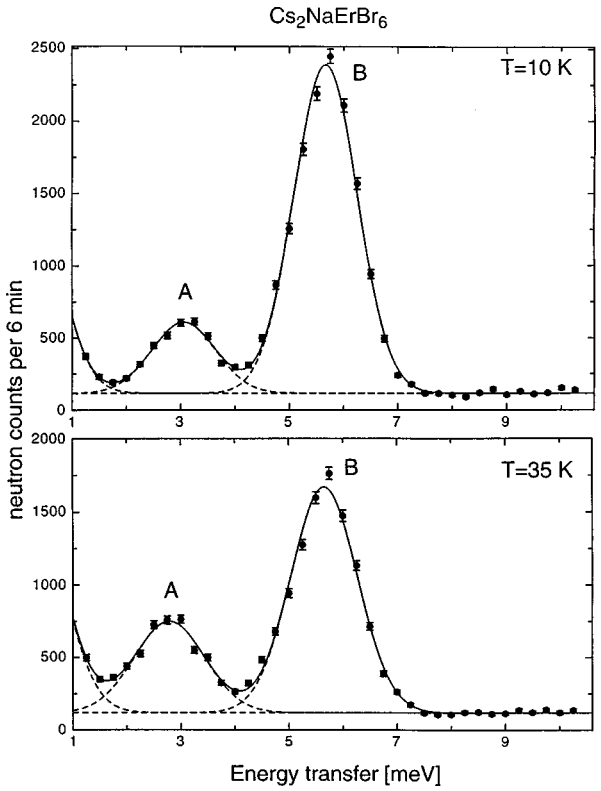

FIG. 12. Low-energy spectra of neutrons scattered from $Cs_2NaErBr_6$. $E_A = 13.7$ meV, $Q = 1.25$ Å^{-1}.

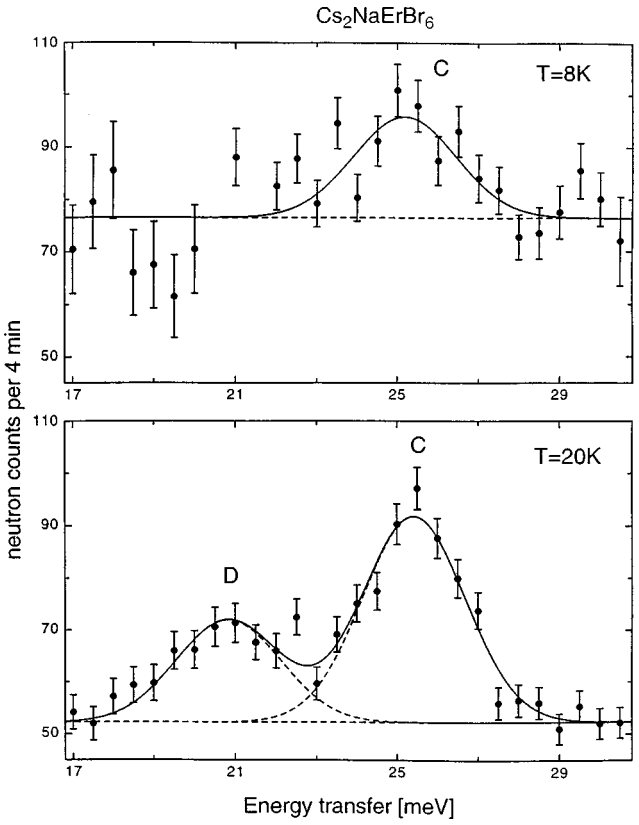

FIG. 13. Medium-energy spectra of neutrons scattered from $Cs_2NaErBr_6$. $E_A = 13.7$ meV, $Q = 2.4$ Å^{-1}.

and the first-excited triplet $\Gamma_4^{(2)}$ as indicated in the inset of Fig. 11. These high-resolution data are allowed to determine the tetragonal CEF parameter B_2^0. The reliability of our analysis is supported by the good agreement between the observed intensity ratio $I_a/I_b/I_c = 0.21/1.00/0.31$ and the ratio 0.20/1.00/0.26 predicted from the CEF model.

H. $Cs_2NaErBr_6$

The cubic CEF splits the 16-fold-degenerate ground-state multiplet $^4I_{15/2}$ of the Er^{3+} ion as for Dy^{3+}, see Sec. V F. The low-temperature spectrum gives evidence for two inelastic lines *A* and *B* at 3.0 and 5.8 meV that can be attributed to the $\Gamma_8^{(1)} \rightarrow \Gamma_7$ and $\Gamma_8^{(1)} \rightarrow \Gamma_8^{(2)}$ ground-state CEF transitions, respectively, see Fig. 12. Upon raising the temperature the intensity of line *B* decreases as expected, whereas the intensity of line *A* increases due to the additional contribution of the excited-state transition $\Gamma_7 \rightarrow \Gamma_8^{(2)}$. The high-lying CEF states Γ_6 and $\Gamma_8^{(3)}$ have very small matrix elements for transitions out of the ground state; thus their energies could only be determined in connection with excited-state transitions (peaks *C* and *D*) as shown in Fig. 13. Thus the CEF level scheme could be completely reconstructed.

I. $Cs_2NaTmBr_6$

The cubic CEF splits the 13-fold-degenerate ground-state *J* multiplet $^3H_6$ of the Tm^{3+} ion as for Tb^{3+}, see Sec. V E. As for $Cs_2NaTbBr_6$ we observe only one ground-state CEF transition (peak *A*) at 5.4 meV (see Fig. 14) which corresponds to the $\Gamma_1 \rightarrow \Gamma_4$ transition. Upon raising the temperature a second line *B* appears at 7.8 meV that can be associated with the $\Gamma_4 \rightarrow \Gamma_5^{(2)}$ transition. Any attempts to locate the remaining three CEF states at higher energies failed, since the corresponding transition matrix elements and/or the thermal population factors were too small to produce well-defined signals. Again, the calculated energies of the high-lying CEF states are included in Fig. 2.

J. $Cs_2NaYbBr_6$

The cubic CEF splits the eightfold-degenerate ground-state multiplet $^2F_{7/2}$ of the Yb^{3+} ion into two doublets Γ_6 and Γ_7 and a quartet Γ_8. The transition between the two doublets is forbidden by the dipole selection rules. In an earlier INS experiment the CEF spectra of the related compound $Cs_2LiYbBr_6$ were presented.[8] Similar energy spectra were observed for the title compound as shown in Fig. 15. In the considered energy-transfer range there are three inelastic lines, but only line *A* at 27 meV exhibits the characteristic form factor behavior expected for CEF transitions. It can be assigned to the $\Gamma_6 \rightarrow \Gamma_8$ ground-state transition. At higher temperatures the excited-state transition $\Gamma_8 \rightarrow \Gamma_7$ (line *B*) shows up as a tiny shoulder on the high-energy side of peak *A*. At $T = 150$ K the observed intensity ratio $I_A/I_B = 10.1 \pm 0.5$ is in excellent agreement with the ratio 10.4 predicted from the CEF model.

VI. DISCUSSION

While there have been many direct spectroscopic determinations of CEF parameters by the INS technique for metallic

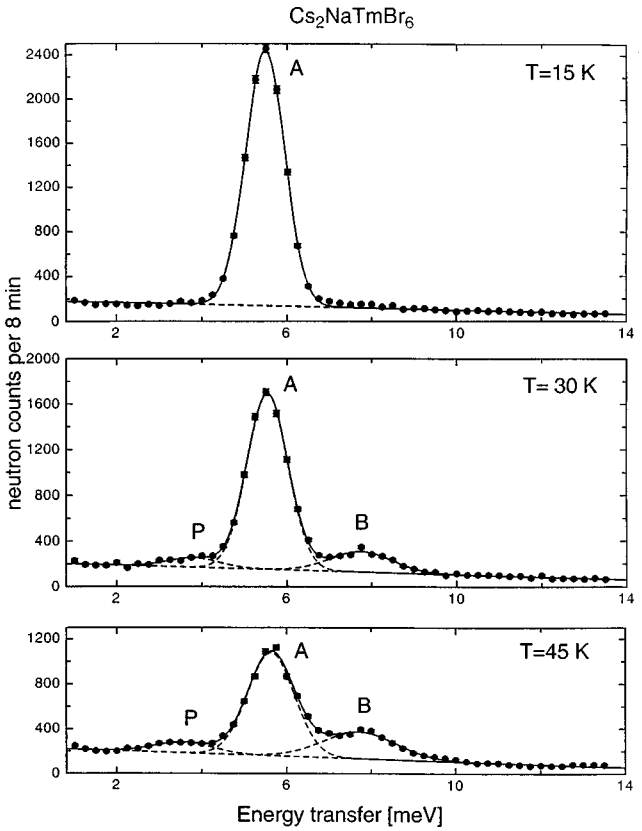

FIG. 14. Low-energy spectra of neutrons scattered from $Cs_2NaTmBr_6$. $E_A = 13.7$ meV, $Q = 1.5$ Å^{-1}.

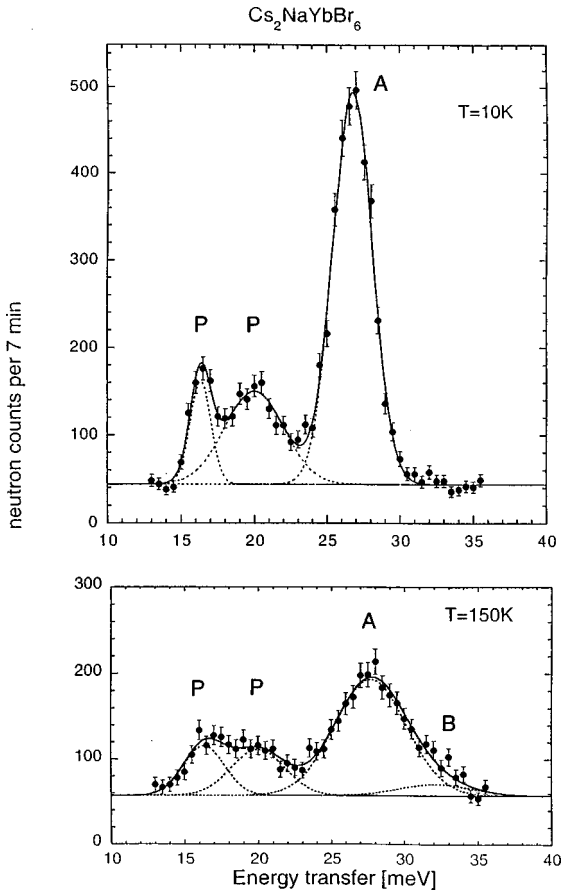

FIG. 15. Medium- and high-energy spectra of neutrons scattered from $Cs_2NaYbBr_6$. $E_A = 15$ meV, $Q = 2.65$ Å^{-1}.

R^{3+} compounds in the past,[30] to our knowledge the present work is the first systematic INS study for insulating systems. The great advantage of the INS technique compared to measurements of bulk properties such as magnetic susceptibility and heat-capacity measurements is that the measurements yield directly the energies of the CEF levels and provide detailed information on the CEF wave functions $|\Gamma_i\rangle$ through the observed transition probabilities; see the cross-section formula (5). CEF splittings of rare-earth compounds in insulators can also be determined by optical absorption and luminescence spectroscopy. These usually have the advantage of higher resolution and allow the determination of CEF states in excited J multiplets. (Due to the copious flux of epithermal neutrons at pulsed spallation sources INS measurements of intermultiplet transitions have recently become possible, see, e.g., Ref. 31.) However, an interpretation of relative intensities requires a much more sophisticated theoretical treatment[32] than presented here for INS experiments. In addition, systems with a center of inversion at the rare-earth site such as the elpasolites reported here suffer from the fact that all optical f-f transitions are electric-dipole forbidden. Optical absorption and luminescence spectra are dominated by vibronic coupling effects and an unambiguous determination of the CEF levels is made difficult.

Absorption and luminescence spectra of bromo-elpasolites have been reported for Cs_2NaRBr_6 (R=Tb, Ho, Tm, Yb) as well as for Pr^{3+}-doped Cs_2NaYBr_6 and Yb^{3+}-doped $Cs_2NaHoBr_6$.[9,10] The agreement with our results is excellent for $Cs_2NaHoBr_6$ with a maximum deviation of 0.5 meV for all seven CEF levels. An equally good agreement is found for $Cs_2NaYbBr_6$. The optically determined splittings associated with the three lowest CEF levels of Pr^{3+}-doped Cs_2NaYBr_6 are systematically smaller by 5–10% than the splittings of $Cs_2NaPrBr_6$ reported here. This can be attributed to the larger unit cell in the doped material. However, there is a discrepancy for the highest CEF level Γ_5, which is located at 55 meV in our INS study, whereas an energy of 76.6 meV was derived from the luminescence spectrum. For $Cs_2NaTmBr_6$ the two techniques are complementary. Both studies place the first-excited CEF level Γ_4 at the same energy. INS gives further information on the second-excited CEF level, whereas the two highest CEF levels have been determined from the luminescence spectrum. For $Cs_2NaTbBr_6$ INS was able to establish the low-energy part of the CEF level structure, whereas no attempts were made to analyze the observed luminescence spectrum in terms of CEF splittings. An erroneous value for the the first-excited CEF level Γ_8 in Yb^{3+}-doped $Cs_2NaHoBr_6$ was obviously derived from the emission spectra. It is in disagreement with both the INS and optical value obtained for $Cs_2NaYbBr_6$. We may conclude that optical and INS techniques both have their merits for the determination of CEF splittings in the electronic ground state of lanthanide compounds.

In the present work we have studied the CEF transitions of the elpasolites Cs_2NaRBr_6 up to about 200 K. Our experi-

TABLE III. Reduced CEF parameters of the elpasolites Cs_2NaRBr_6.

R	A_2a^3 (10^4 meV Å)	A_4a^5 (10^7 meV Å)	A_6a^7 (10^7 meV Å)
Ce		1.20±0.02	
Pr		0.99±0.07	8.4±0.8
Nd		1.66±0.05	8.5±0.4
Tb		1.9±0.2	12±3
Dy	−1.4±0.2	2.6±0.2	15±3
Ho	−0.9±0.3	2.4±0.2	13±2
Er		2.6±0.1	11±1
Tm		2.7±0.4	11±2
Yb		2.9±0.1	12±3

TABLE IV. Easy axes of magnetization and saturated magnetic moments μ_{sat} in zero magnetic field predicted for the Cs_2NaRBr_6 compounds. The tetragonal axis is [001].

R	Easy axis of magnetization	μ_{sat} (μ_B)
Ce	⊥[001]	0.83
Pr	⊥[001]	0
Nd	[100] or [010]	2.94
Tb	[111]	0
Dy	[100] or [010]	2.50
Ho	[100] or [010]	0
Er	[101] or [011]	5.06
Tm	[111]	0
Yb	[001]	1.16

ments reveal practically no temperature dependence of the CEF energies, but the CEF transitions exhibit considerable line broadening with increasing temperature, similar to the behavior of CEF excitations in metallic R^{3+} systems. The likely origin of the line broadening observed for the bromo-elpasolites is the thermal motion of the coordination polyhedra built by the Br^- ligand ions around the R^{3+} sites, whereas in metallic systems the renormalization effects are predominantly due to the conduction electrons.

In order to explore the behavior of the CEF parameters in the whole Cs_2NaRBr_6 series, we try to correlate our results in terms of reduced CEF parameters:

$$A_n a^{n+1} = \frac{B_n a^{n+1}}{\langle r^n \rangle \chi_n}, \tag{6}$$

where a is the lattice constant (see Table I), $\langle r^n \rangle$ the relativistic free-ion radial integral of the $4f$ electrons,[33] and χ_n the reduced matrix element.[25,26] Equation (6) takes account of the lanthanide contraction, so that we expect the nth-order reduced CEF parameter to be constant throughout the rare-earth series as long as the charge distribution around the R^{3+} sites is not changed. Table III lists the reduced CEF parameters derived for the elpasolites Cs_2NaRBr_6. The hierarchy $|A_2a^3| \ll A_4a^5 < A_6a^7$ readily reflects the interaction range expected for the CEF parameters in ionic systems that changes from very long range for the second-order to short range for the sixth-order CEF parameters. The reduced fourth- and sixth-order CEF parameters are found to increase somewhat by going from the light to the heavy rare-earth ions, similar to CEF results for metallic systems.[34] This effect has been thoroughly investigated and discussed for the isostructural chloro-elpasolites in terms of dipolar polarizability and covalency,[20,22] which seem to have an increased relative importance for the heavy rare-earth compounds.

For most Cs_2NaRBr_6 compounds studied in this work the CEF interaction of octahedral symmetry exerts a strong anisotropy on the R^{3+} ions and therefore has an essential influence on the magnetic properties. This effect manifests itself in the anisotropy of the g factor, which can be calculated from the CEF parameters in a straightforward manner (e.g., by calculating the magnetic moments of the R^{3+} ions induced by an external magnetic field applied along different symmetry directions). The anisotropy of the g factor determines then immediately the easy axes of magnetization. Only for R=Ce, Pr, and Yb is the anisotropy of the octahedral CEF very weak giving rise to essentially isotropic g factors. In these cases the magnetic behavior is controlled by the tetragonal component of the CEF interaction. Based on the results obtained for R=Dy and Ho (see Tables II and III) we have been able to extrapolate the sign of the tetragonal CEF parameters B_2^0 for the remaining members of the bromo-elpasolite series according to Eq. (6). The magnetic properties of the Cs_2NaRBr_6 compounds derived from our CEF results are summarized in Table IV, which lists the predicted easy axes of magnetization as well as the saturated magnetic moments μ_{sat} of the R^{3+} ions in zero magnetic field. The values of μ_{sat} are, throughout, drastically reduced below the corresponding free-ion values and are obviously zero for all compounds with a singlet CEF ground state. This information will be useful in forthcoming studies of the long-range magnetic order at milli-Kelvin temperatures due to dipolar forces which have already been started for the isostructural chloro-elpasolite series.[23]

Finally, we discuss whether the results obtained for the bromo-elpasolites in the present work can be applied to predict the CEF potential of the isostructural compounds Cs_2NaRX_6 (X=F, Cl). The CEF splitting patterns reported for the chloro-elpasolites[8,21] are very similar to the corresponding bromo-elpasolites presented here, i.e., the CEF transitions are simply shifted to higher energies by 15–30 % as expected from the smaller bond length between the rare-earth and ligand ions. As a result the CEF parameters of the Cl compound series are enhanced typically by 30% for B_4 which is exactly what is expected by taking into account the lattice contraction [see Eq. (6)], but only by 15% for B_6 whereas 40% are predicted by Eq. (6). Obviously, there are subtle differences in the charge distribution between the bromo- and chloro-elpasolites, which predominantly affect the sixth-order term of the CEF potential. Nevertheless, the fourth-order term is by far dominating the CEF potential, which means that in spite of the slight discrepancy with the sixth-order term the reduced CEF parameters listed in Table III may serve as a useful extrapolation scheme for other isostructural elpasolites, at least to an accuracy of about 10%. The reduced CEF parameters can also be used as a convenient interpolation scheme to predict the CEF interaction for those rare-earth elpasolites not included in the present study

(Pm: rapid radioactive decay to Sm; Sm, Eu, Gd: high-absorption cross-section for neutrons, the latter two R^{3+} ions are *S*-state ions and have, therefore, no CEF splitting in the ground-state *J* multiplet in first order; moreover, the Stevens's operator equivalents technique cannot be applied, but a full *J* mixing and intermediate coupling calculation involving the higher *J* multiplets as, e.g., described in Ref. 21 has to be performed).

ACKNOWLEDGMENTS

Financial support by the Swiss National Science Foundation is gratefully acknowledged. We are indebted to N. Furer for preparing most of our samples as well as to A. Hartmann and U. Gasser for technical assistance with the figures. We thank Dr. P. Allenspach and Dr. J. Mesot for helpful discussions and critical reading of the manuscript.

[1] A. Furrer, H. U. Güdel, H. Blank, and A. Heidemann, Phys. Rev. Lett. **62**, 210 (1989).
[2] A. Furrer, H. U. Güdel, E. R. Krausz, and H. Blank, Phys. Rev. Lett. **64**, 68 (1990).
[3] H. U. Güdel, A. Furrer, and H. Blank, Inorg. Chem. **29**, 4081 (1990).
[4] M. A. Aebersold, H. U. Güdel, A. Hauser, A. Furrer, H. Blank, and R. Kahn, Phys. Rev. B **48**, 12 723 (1993).
[5] M. A. Aebersold, H. U. Güdel, A. Furrer, and H. Blank, Inorg. Chem. **33**, 1133 (1994).
[6] G. Meyer and H. C. Gaebell, Z. Naturforsch. B **33**, 1476 (1978).
[7] G. Meyer, Inorg. Synth. **22**, 1 (1983).
[8] A. Furrer, H. U. Güdel, and J. Darriet, J. Less-Common Met. **111**, 223 (1985).
[9] P. A. Tanner, V. V. Ravi Kanth Kumar, C. K. Jayasankar, and M. F. Reid, J. Alloys Compd. **215**, 349 (1994), and references cited therein.
[10] A. J. Berry, C. S. McCaw, I. D. Morrison, and R. G. Denning, J. Lumin. **66&67**, 272 (1996).
[11] W. Bührer and H. U. Güdel, J. Phys. C **20**, 3809 (1987).
[12] I. N. Flerov, W. Bührer, M. V. Gorev, H. U. Güdel, and A. E. Usachev, J. Phys.: Condens. Matter **2**, 9019 (1990).
[13] D. G. Karraker, J. Chem. Phys. **55**, 1084 (1971).
[14] B. D. Dunlap and G. K. Shenoy, Phys. Rev. B **12**, 2716 (1975).
[15] B. C. Tofield and H. P. Weber, Phys. Rev. B **10**, 4560 (1974).
[16] R. W. Schwartz, Inorg. Chem. **16**, 1694 (1977).
[17] L. C. Thompson, O. A. Serra, J. P. Riehl, F. S. Richardson, and R. W. Schwartz, Chem. Phys. **26**, 393 (1977).
[18] H. D. Amberger, G. G. Rosenbauer, and R. D. Fischer, Mol. Phys. **32**, 1291 (1976), and references 7, 8, and 14 cited therein.
[19] B. Kanellakopoulos, H. D. Amberger, G. G. Rosenbauer, and R. D. Fischer, J. Inorg. Nucl. Chem. **39**, 607 (1977).
[20] T. R. Faulkner, J. P. Morley, F. S. Richardson, and R. W. Schwartz, Mol. Phys. **40**, 1481 (1980).
[21] F. S. Richardson, M. F. Reid, J. L. Dallara, and R. D. Smith, J. Chem. Phys. **83**, 3813 (1985).
[22] M. F. Reid and F. S. Richardson, J. Chem. Phys. **83**, 3831 (1985).
[23] M. R. Roser, J. Xu, S. J. White, and L. R. Corruccini, Phys. Rev. B **45**, 12 337 (1992).
[24] K. W. H. Stevens, Proc. Phys. Soc. London, Sect. A **65**, 209 (1952).
[25] M. T. Hutchings, in *Solid State Physics*, edited by F. Seitz and D. Turnbull (Academic, New York, 1964), Vol. 16, p. 227.
[26] K. R. Lea, M. J. M. Leask, and W. P. Wolf, J. Phys. Chem. Solids **23**, 1381 (1962).
[27] F. Lévy, Phys. Kondens. Mater. **10**, 85 (1969).
[28] G. T. Trammell, Phys. Rev. **92**, 1387 (1953).
[29] R. J. Birgeneau, J. Phys. Chem. Solids **33**, 59 (1972).
[30] See, e.g., U. Walter and E. Holland-Moritz, Z. Phys. B **45**, 107 (1981).
[31] M. Guillaume, W. Henggeler, A. Furrer, R. S. Eccleston, and V. Trounov, Phys. Rev. Lett. **74**, 3423 (1995).
[32] G. W. Burdick, C. K. Jayasankar, F. S. Richardson, and M. F. Reid, Phys. Rev. B **50**, 16 309 (1994).
[33] W. B. Lewis, in *Proceedings of the XVI Annual Congress AMPERE*, edited by I. Ursu (Publishing House of the Academy, Bucharest, 1971), p. 717.
[34] R. J. Birgeneau, E. Bucher, J. P. Maita, L. Passell, and K. C. Turberfield, Phys. Rev. B **8**, 5345 (1973).